Electronic supporting information

Spin-crossover iron (II) complex showing thermal hysteresis around room temperature with symmetry breaking and an unusually high *T*(LIESST) of 120 K.

Víctor García-López, [a] Mario Palacios-Corella, [a] Salvador Cardona-Serra,[a] Miguel Clemente-León*[a] and Eugenio Coronado [a]

[a] *Instituto de Ciencia Molecular (ICMol), Universidad de Valencia, Catedrático José Beltrán 2, 46980 Paterna, Spain.*

ESI. 1 Experimental section.

ESI. 2 Structural characterization.
Table S1. Crystallographic data

ESI. 3 Differential scanning calorimetry (DSC)
Fig. S1 Differential scanning calorimetry of **1**.

ESI. 4 Magnetic characterization.
Fig. S2 Thermal dependence of χ_MT of **1** measured in contact with the mother liquor (empty circles) and dry sample after heating to 400 K (full blue circles).

ESI. 5 Powder X-ray diffraction (PRXD).
Fig. S3 PXRD patterns of **1** at 300 K in contact with the mother liquor (blue), filtered (green), and simulated one from the single crystal structure at 300 K (red).
Fig. S4 Thermal dependence of the experimental PXRD pattern of **1** (top) and simulated one (bottom) from the single crystal structure at 120 and 300 K.
Fig. S5 PXRD pattern of **1** at 290 K (blue), 250 K (red) and 290 K after cooling to 250 K (black) to confirm reversibility of the crystallographic symmetry breaking.

ESI. 6 Structure.
Fig. S6 Hydrogen bond interactions of $[Fe(bpCOOH_2p)_2]^{2+}$ complexes (blue-dashed lines) in the structure of **1** at 120 K (a) and 300 K (b and c).
Fig. S7 Chains of $[Fe(bpCOOH_2p)_2]^{2+}$ complexes linked through intermolecular interactions (red-dashed lines) in the structure of **1** at 120 K (a) and 300 K (b and c).
Fig. S8 Interchain interactions between $[Fe(bpCOOH_2p)_2]^{2+}$ complexes (red-dashed lines) in the structure of **1** at 300 K.

ESI. 7 Photomagnetism and theoretical evaluation of the kinetic relaxation.
Fig. S9 Temperature dependence of the first derivative of χ_MT with respect to the temperature of **1** after light irradiation with red light.
Fig. S10 (Left) Time dependence at various temperatures of the photoinduced HS molar fraction. The relaxation curves are fitted according to sigmoidal behavior (see text for more details). (Right) Arrhenius fitting of the activate process (the measurement at 105K has been removed from the fitting, see text).
Fig. S11 Thermal dependence of χ_MT of **1**. Full squares: data recorded without irradiation; Black empty circles: data recorded after the first irradiation at 10 K and; Red empty circles: data recorder after second irradiation at 10 K.

ESI. 8 Structure and magnetic properties of 2.
Fig. S12 Structure of the $[Fe^{II}(bpCOOH_2p)(bpCOOCOOHp)Fe^{II}(bpCOOH_2p)(ClO_4)]^{2+}{}_n$ chains in the structure of **2** at 120 K. Fe (orange) C (black), N (blue), O (red), Cl (yellow), H(white).
Fig. S13 Thermal dependence of χ_MT of **2**. Empty circles: Compound measured in contact with the mother liquor. Full squares: data recorded without irradiation after desolvation at 400 K; red empty circles: data recorded after irradiation at 10 K for the same desolvated sample.

ESI. 1 Experimental section.

Experimental

The 2,6-di[4-(ethylcarboxy)pyrazol-1-yl]pyridine ester ($bpCOOEt_2p$) was prepared as reported in the literature.[1] All other chemicals are commercially available and were used as received without further purification.

Synthesis of $bpCOOH_2p$.

This ligand was synthesized by a saponification with aqueous NaOH of the ester $bpCOOEt_2p$ adapting the method reported in the literature for the preparation of 2,6-Dibromopyridine-4-carboxylic Acid.[2] Aqueous NaOH (1.2 mM, 9.4 mL) was added to $bpCOOEt_2p$ (530mg, 1.5mmol) in 10mL of THF, and the mixture was refluxed for 5 h. THF was removed under vacuum and 10mL of water were added. The solution was acidified with HCl (3M) to pH 1.5. The white solid obtained was filtered and washed with water. Yield 375 mg, 84 %. ^{1}H NMR (400 MHz, ppm in dimethyl sulfoxide-d_6): 7.94 (dd, 2H), 8.15-8.30 (m, 3H), 9.61 (d, 2H).

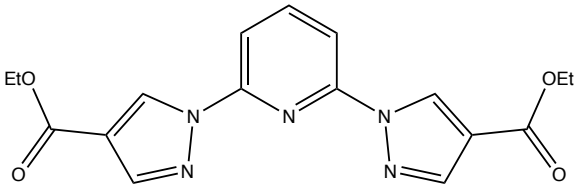

Scheme S1. $bpCOOEt_2p$

Synthesis of $[Fe^{II}(bpCOOH_2p)_2](ClO_4)_2\cdot 3.5Me_2CO$ (1) and $[Fe^{II}(bpCOOCOOHp)(bpCOOH_2p)Fe^{II}(bpCOOH_2p)(ClO_4)](ClO_4)_2\cdot 1.5H_2O\cdot 1.5Me_2CO$ (2).

CAUTION: perchlorate salts are explosive when heated or subjected to friction.

$Fe(ClO_4)_2\cdot xH_2O$ (9 mg, 0.025 mmol) in acetone (1.5 mL) was added to a solution of bpCOOHp (15 mg, 0.05 mmol) in acetone (1.5 mL) inside the N_2 atmosphere of a glove box. The mixture was stirred for 15 minutes and filtered. A yellow solution was obtained. Orange prismatic crystals of $[Fe(bpCOOHp)_2](ClO_4)_2\cdot 3.5Me_2CO$ (**1**) suitable for X-ray diffraction were obtained by slow diffusion of diethyl ether into this solution in a narrow tube (diameter 0.5 cm) after one week inside the glove box. If the diffusion tubes were placed in an air atmosphere after this time, the crystals of **1** dissolved and yellow rectangular crystals of **2** suitable for X-ray diffraction appeared after several weeks. Yield 2 mg, 7 % (**1**) and 3 mg, 8 % (**2**). The composition of crystals of **1** and **2**, checked by microanalysis, shows a Fe:Cl ratio close to 1:2 and 2:3, respectively. Elemental analysis of filtered samples of **1** and **2** is more consistent with the presence of four and five water molecules. This suggests loss of acetone molecules and absorption of water molecules after filtering the crystals. $[Fe^{II}(bpCOOH_2p)_2](ClO_4)_2\cdot Me_2CO\cdot 4H_2O$ (983.37) (**1**): calcd. C 35.42, N 14.24, H 3.28; found C 35.37, N 14.61, H 2.93. $[Fe^{II}(bpCOOCOOHp)(bpCOOH_2p)Fe^{II}(bpCOOH_2p)(ClO_4)](ClO_4)_2\cdot 5H_2O$ (1396.835) (**2**): calcd. C 33.53, N 15.04, H 2.60; found C 33.53, N 14.98, H 2.50.

Physical characterization.

The Fe/Cl ratios were measured with a Philips ESEM X230 scanning electron microscope equipped with an EDAX DX-4 microsonde. Elemental analyses (C, H, and N) were performed with a CE Instruments EA 1110 CHNS Elemental analyzer.

Differential scanning calorimetry (DSC) measurements under nitrogen atmosphere were performed in a Mettler Toledo DSC 821e apparatus with warming and cooling rates equal to 2 $K\cdot min^{-1}$. A correction from the sample holder was automatically applied. The heat flow thus measured ($\Delta H/\Delta t$) was used in the calculation of the approximate specific heat function as follows:

$$\frac{\Delta H}{\Delta T} = \frac{\Delta H}{\Delta t}\cdot\frac{M}{\beta\cdot m}$$

where m is the mass of the sample, M its molecular weight and β the heating (cooling) rate.

Magnetic measurements were performed with a Quantum Design MPMS-XL-5 SQUID magnetometer in the 2 to 400 K temperature range with an applied magnetic field of 0.1 T at a scan rate of 1 K/min (0.5 for **1**) on a polycrystalline sample. To avoid desolvation, crystals of **1** were deposited in the bottom of a glass tube and covered with the mother liquor. This tube was used as the sample holder. 5.2 mg of **1**

were used for this measurement. Photomagnetic measurements were performed irradiating with a 30993 cylindrical Helium-Neon Laser system from Research Electro-Optics (red light, λ = 633 nm, optical power 12 mW cm^{-2}) and a Diode Pumped Solid State Laser DPSS-532-20 from Chylas (green light, λ = 532 nm, optical power 3.4 mW cm^{-2}) coupled via an optical fiber to the cavity of the SQUID magnetometer. It was verified that irradiation resulted in no significant change in magnetic response due to heating of the sample. The photomagnetic samples consisted of a thin layer of compound whose weight was corrected by comparison of a thermal spin crossover curve with that of a more accurately weighted sample of the same compound.

ESI. 2 Structural characterization.

Single crystals of **1** and **2** were mounted on a glass fiber using a viscous hydrocarbon oil to coat the crystal and then transferred directly to the cold nitrogen stream for data collection. X-ray data were collected at 120 (**1** and **2**) and 300 K (**1**) on a Supernova diffractometer equipped with a graphite-monochromated Enhance (Mo) X-ray Source (λ = 0.71073 Å). Higher temperatures leaded to the quick loss of crystallinity of **1**. The program CrysAlisPro, Oxford Diffraction Ltd., was used for unit cell determinations and data reduction. Empirical absorption correction was performed using spherical harmonics, implemented in the SCALE3 ABSPACK scaling algorithm. The structures of were solved with the ShelXT structure solution program[3] and refined with the SHELXL-2013 program,[4] using Olex2.[5] Non-hydrogen atoms were refined anisotropically, and hydrogen atoms were placed in calculated positions refined using idealized geometries (riding model) and assigned fixed isotropic displacement parameters. In **2** as it was not possible to see clear electron-density peaks in difference maps which would correspond with acceptable locations for the various H atoms bonded to oxygen atoms, the refinement was completed with no allowance for these H atoms in the model. They have been included in chemical formula in the cif file and table S1. Crystallographic data are summarized in Table S1. CCDC-1944600-1944602 contain the supplementary crystallographic data for this paper. These data can be obtained free of charge from The Cambridge Crystallographic Data Centre via www.ccdc.cam.ac.uk/data_request/cif. For X-Ray powder pattern, a 0.5 mm glass capillary was filled with a polycrystalline sample of de complexes and mounted and aligned on an Empyrean PANalytical powder diffractometer, using CuKα radiation (λ = 1.54177 Å). A total of 2 scans were collected at room temperature in the 2θ range 5-40º.

Table S1. Crystallographic data

Compound	**1**	**1**	**2**
Empirical formula	$C_{36.5}H_{39}Cl_2FeN_{10}O_{19.5}$	$C_{73}H_{78}Cl_4Fe_2N_{20}O_{39}$	$C_{87}H_{74}Cl_6Fe_4N_{30}O_{53}$
Formula weight	1056.53	2113.05	2823.86
Crystal color	Brown-orange	Orange	Yellow
Temperature (K)	120	300	120
Wavelength (Å)	0.71073	0.71073	0.71073
Crystal system, Z	Monoclinic, 4	Triclinic, 2	Triclinic, 1
Space group	$P2_1/c$	P-1	P-1
a (Å)	19.2527(3)	12.8517(4)	14.6268(6)
b (Å)	17.9600(3)	18.4107(4)	15.0615(6)
c (Å)	12.8378(2)	19.5908(4)	15.2862(6)
α (º)	90	88.715(2)	96.056(3)
β (º)	91.571(2)	88.876(2)	112.125(4)
γ (º)	90	89.761(2)	104.778(4)
V (Å^3)	4437.37(12)	4633.2(2)	2939.0(2)
ρcalc (Mg/m^3)	1.581	1.473	1.595
μ(Mo$_{K\alpha}$) (mm^{-1})	0.552	0.525	0.728
2θ range (°)	6.638 to 55.032	6.636 to 55.072	6.612 to 56.02
Reflns collected	32411	64980	43662
Independent reflns, (R_{int})	9404 (0.0466)	19501 (0.0904)	12366 (0.0880)
L. S. parameters/ restraints	631/2	1260 /43	902/8
R1(F),[a] I>2σ(I)]	0.0515	0.0817	0.0952
wR2(F^2),[b] all data	0.1291	0.2635	0.3065
S(F^2),[c] all data	1.040	1.046	1.030

[a] $R1(F) = \sum(||F_O| - |F_C||)/\sum|F_O|$; [b] $wR2(F^2) = [\sum w(F_O^2 - F_C^2)^2/\sum wF_O^4]^{1/2}$; [c] $S(F^2) = [\sum w(F_O^2 - F_C^2)^2/(n - p)]^{1/2}$.

ESI. 3 Differential scanning calorimetry (DSC)

An exothermic peak at 286 K upon cooling and an endothermic peak at 297 K in the heating mode are observed (See Fig. S1). There is a shift of around 5 K to higher temperatures with respect to the magnetic measurements, which could be related to the different method used to protect the crystals (oil in DSC and mother liquor in magnetic measurements) and to the different scan rate in both measurements.

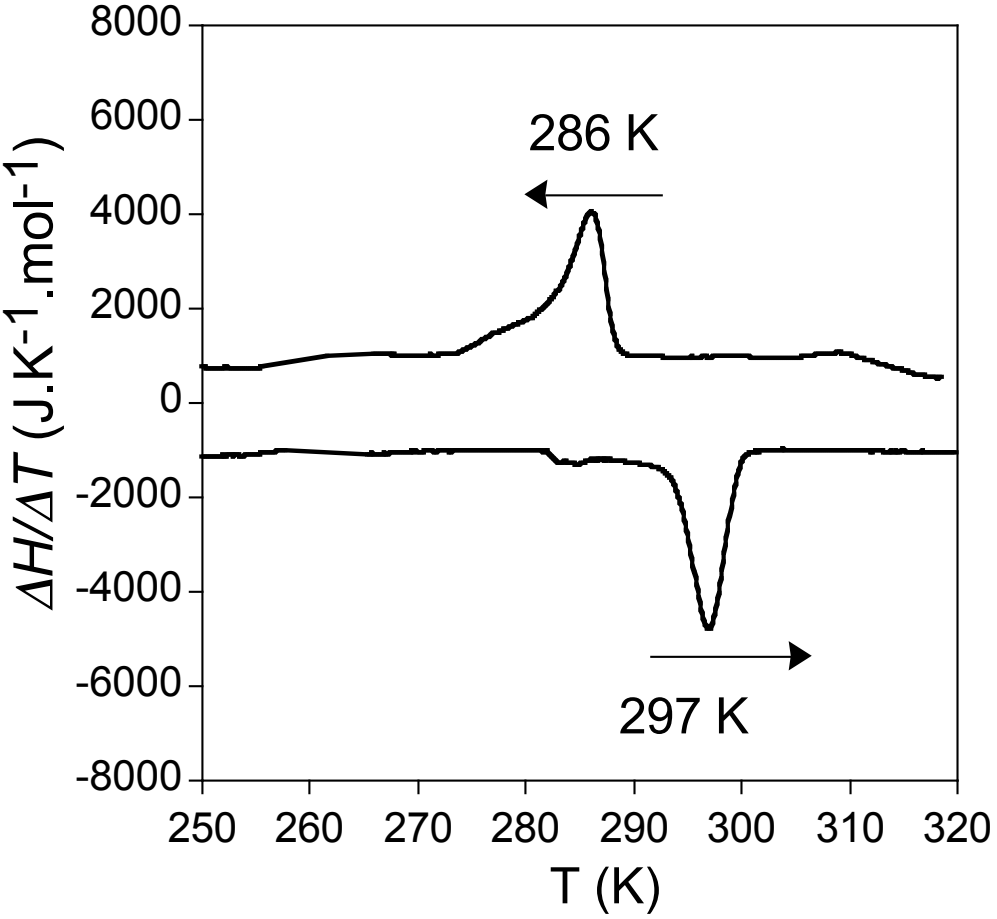

Fig. S1 Differential scanning calorimetry of **1**.

ESI. 4 Magnetic characterization.

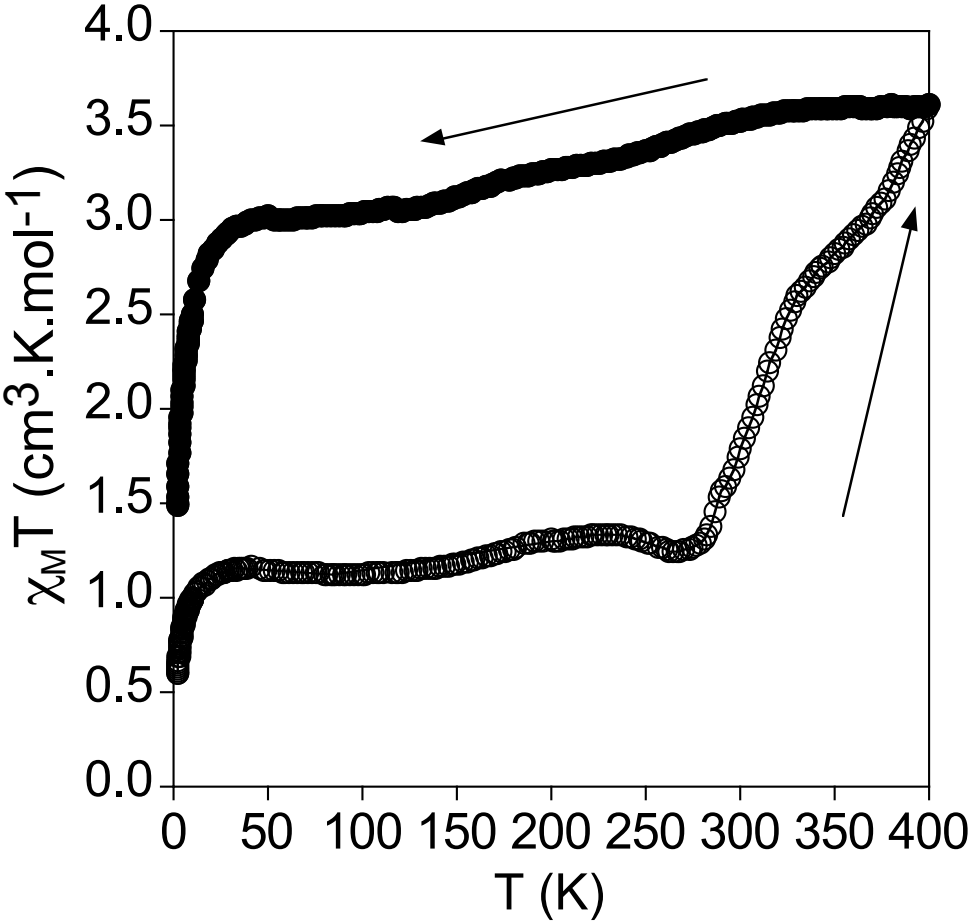

Fig. S2 Thermal dependence of $\chi_M T$ of dried crystals of **1** in the first heating cycle (empty circles) and after being heated to 400 K (full circles).

$\chi_M T$ of dried crystals of **1** shows a value close to 1.2 $cm^3 \cdot K \cdot mol^{-1}$ from 50 to 300 K. Above this temperature, it increases abruptly and irreversibly to reach a value of 3.6 $cm^3 \cdot K \cdot mol^{-1}$ at 400 K, which corresponds to 100 % of the molecules in the HS state. This value remains almost constant when the sample is successively cooled from 400 to 2 k with a decrease below 30 K due to zero-field-splitting of HS Fe(II). This suggests that desolvation leads to irreversible structural changes that stabilize the HS state as confirmed by powder X-ray diffraction (PXRD) data (see Fig. S3). On the other hand, the value of 1.1 $cm^3 \cdot K \cdot mol^{-1}$ obtained before heating to 400 K could indicate a mixture of different solvates and desolvated crystals. We have to take into account that PXRD of dried crystals shows a loss of crystallinity (see Fig. S3). Furthermore, elemental analysis of dried crystals is more consistent with the presence of one Me_2CO and four H_2O per molecule instead of the 3.5 Me_2CO molecules found in he structure (see experimental section).

ESI. 5 Powder X-ray diffraction (PRXD).

PXRD pattern at 300 K measured in contact with the mother liquor agrees with the simulated one from the single crystal structure at this temperature (see Fig. S3). The crystallographic symmetry breaking was also monitored by PXRD experiments at different temperatures. Thus, the sample was first measured at 290 K and then cooled to 250 K to reach the LS phase, and then another PXRD pattern was collected again at 290 K to confirm reversibility (Fig. S4 and S5). The two diffractograms at 290 K and that at 250 K are in good agreement with simulated powder patterns for the P-1 and $P2_1/c$ phases, respectively (Fig. S4), with some differences related to the different temperature of the experimental $P2_1/c$ pattern (250 K) and the simulated one (120 K). PXRD pattern at room temperature of filtered crystals presents important differences with respect to the simulated one confirming that the loss of crystallinity observed in single crystal measurements above 300 K is related to the loss of solvent molecules (Fig. S3). Indeed, elemental analysis of a filtered sample of **1** is more consistent with the presence of one acetone and four water molecules (see experimental section). This suggests partial loss of acetone molecules and absorption of water molecules after filtering the crystals.

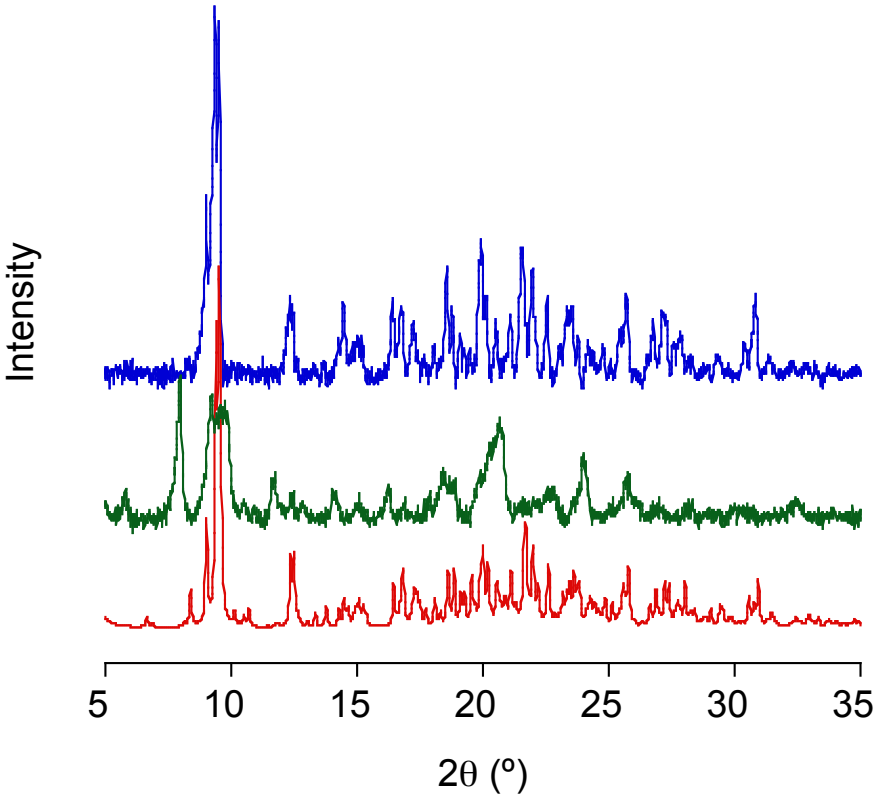

Fig. S3 PXRD patterns of **1** at 300 K in contact with the mother liquor (blue), dried sample (green), and simulated one from the single crystal structure at 300 K (red).

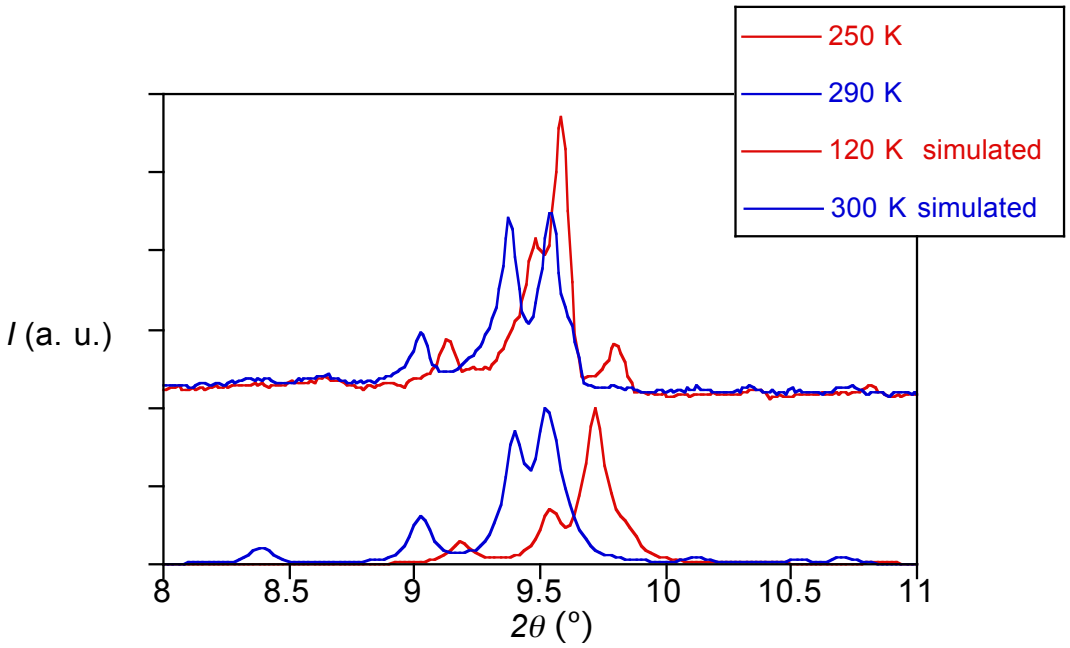

Fig. S4 Thermal dependence of the experimental PXRD pattern of **1** (top) and simulated one (bottom) from the single crystal structure at 120 and 300 K.

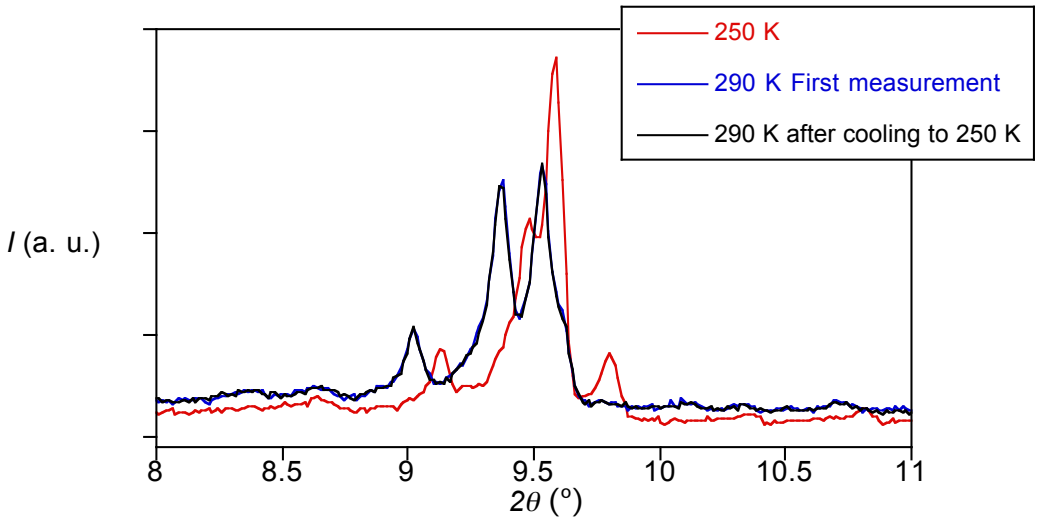

Fig. S5 PXRD pattern of **1** at 290 K (blue), 250 K (red) and 290 K after cooling to 250 K (black) to confirm reversibility of the crystallographic symmetry breaking.

ESI. 6 Structure of 1.

The unit cell of **1** contains one crystallographically independent $[Fe(bpCOOH_2p)_2]^{2+}$ cation, two perchlorate counteranions and four acetone molecules (one of them with an occupancy of 0.5) at 120 K. At 300 K, there are two crystallographically independent $[Fe(bpCOOH_2p)_2]^{2+}$ cations (with Fe1 and Fe2), four perchlorate counteranions and six acetone molecules. One of these acetone and perchlorate molecules are disordered at 300 K. Furthermore, in the structure of **1** at 300 K, there are solvent accesible voids. The subroutine SQUEEZE was used to calculate the diffracting component of disordered solvents resulting in a void of ca. 186 $Å^3$ and 28 electrons/cell.[6] This corresponds to ca. one acetone molecule per cell. This molecule has been included in the molecular formula of the cif file leading to the same formula obtained in the structure at 120 K.

Packing of $[Fe(bpCOOH_2p)_2]^{2+}$ complexes. At 120 K, neighboring $[Fe(bpCOOH_2p)_2]^{2+}$ cations present $\pi\cdots\pi$ interactions between the pyrazolyl rings and several short contacts involving the CO groups of the carboxylic acid groups. This gives rise to chains of complexes along the *c* axis (see Fig. S7). At 300 K, there are two types of chains, which now run along the *a* axis. Chains of LS $[Fe(bpCOOH_2p)_2]^{2+}$ cations with Fe1 present similar interactions to those at 120 K (see Fig. S7). In contrast to this, the HS $[Fe(bpCOOH_2p)_2]^{2+}$ cations with Fe2 form chains with a smaller number of intermolecular interactions. Thus, $\pi\cdots\pi$ interactions are not observed due to an increase of the C···C distances between pyrazolyl rings of neighboring complexes related by an inversion center ($d_{C41\cdots C41}$ = 3.416 Å for HS complexes and $d_{C2\cdots C2}$ = 3.288 Å for LS complexes). At the same time, the number of short contacts involving the CO groups decreases (see Fig. S7). These chains are linked at 120 K through several contacts involving O atoms from carboxylic acid groups and CH groups from pyridine and pyrazole leading to a double layer of complexes in the *bc* plane (see Fig. 1). Similar double layers of complexes in the *ab* plane are found in the structure at 300 K but complexes with Fe1 and Fe2 belonging to different chains present stronger interactions (see Fig. S8).

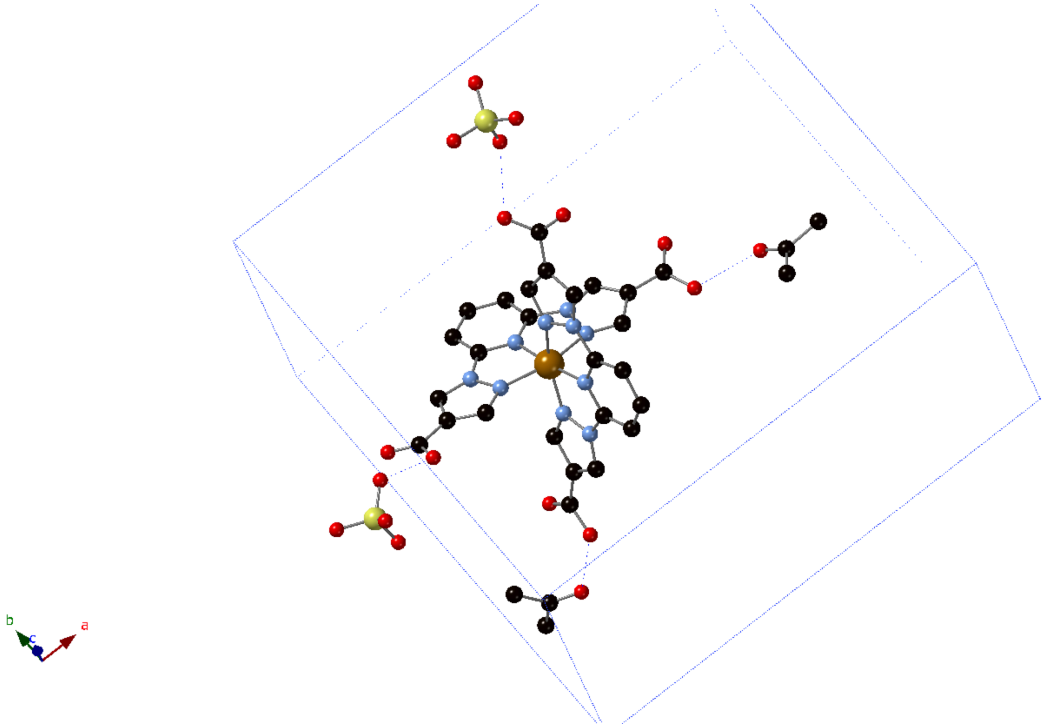

(a)

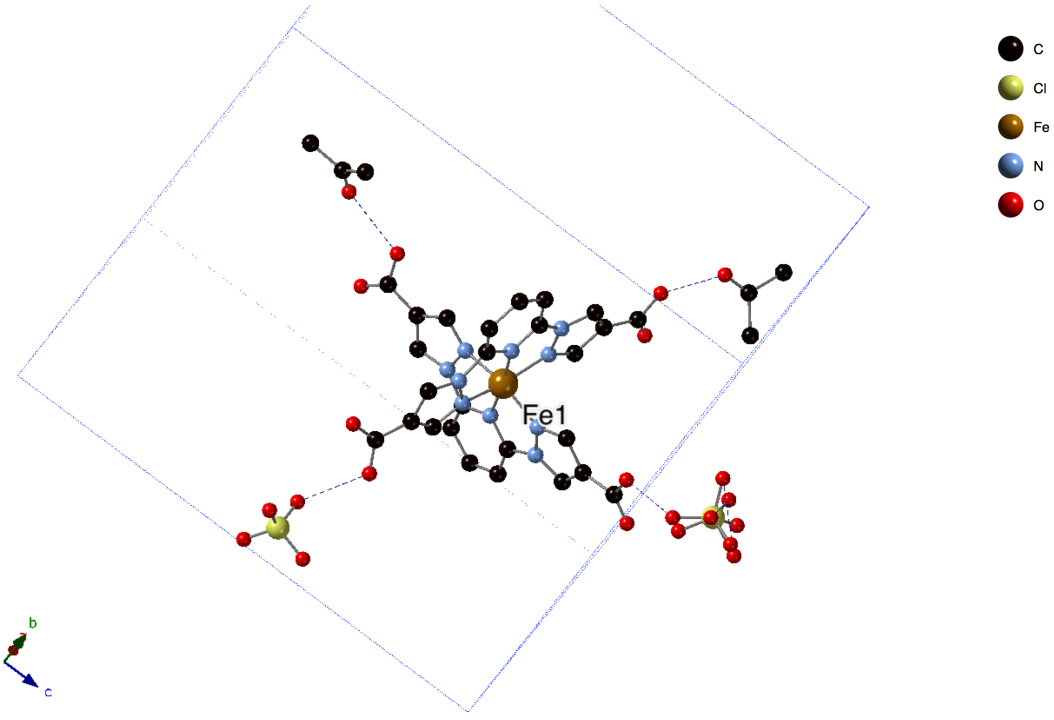

(b)

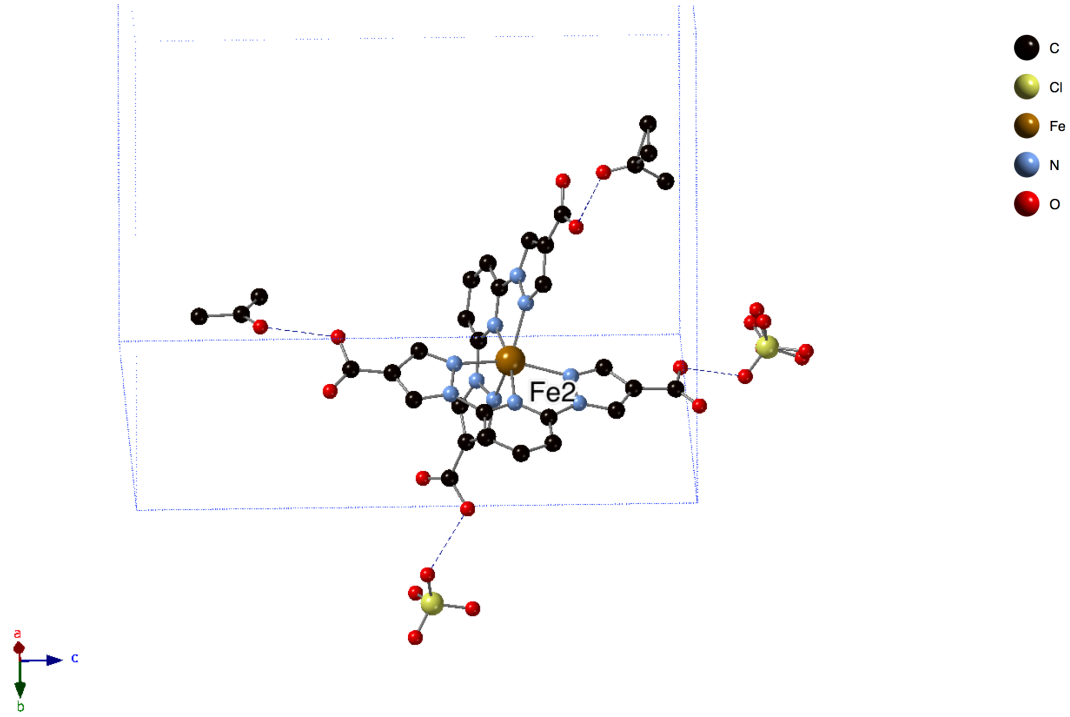

(c)

Fig. S6 Hydrogen bond interactions of $[Fe(bpCOOH_2p)_2]^{2+}$ complexes (blue-dashed lines) in the structure of **1** at 120 K (a) and 300 K (b and c).

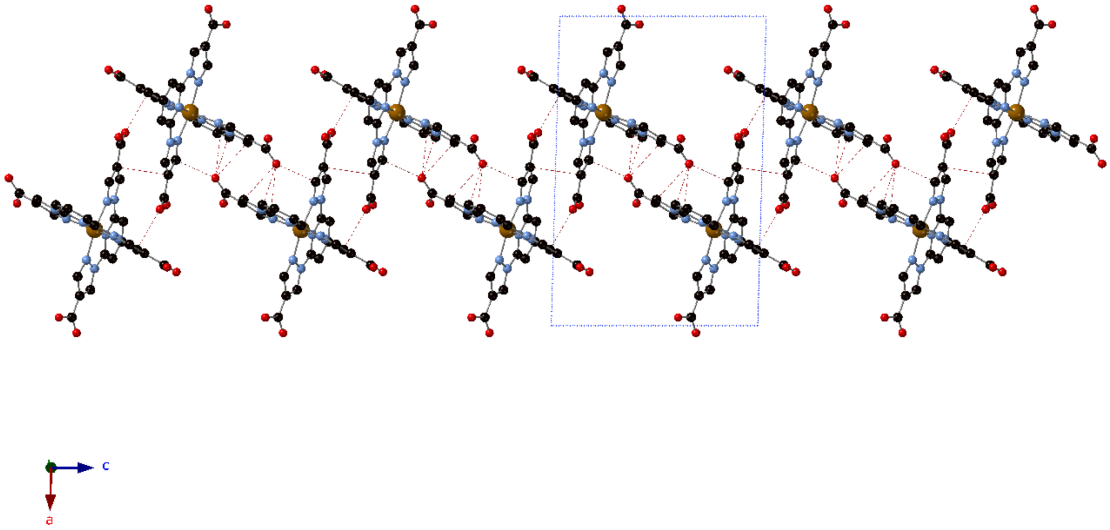

(a)

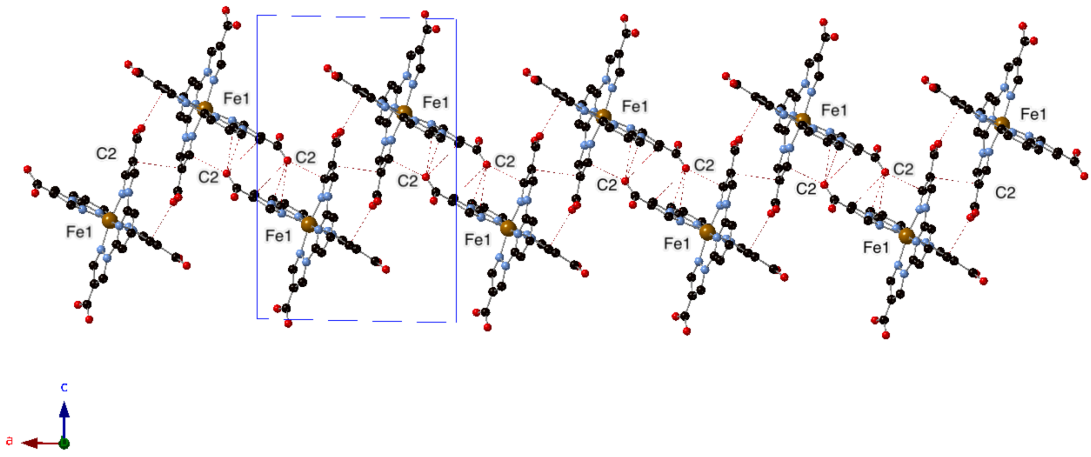

(b)

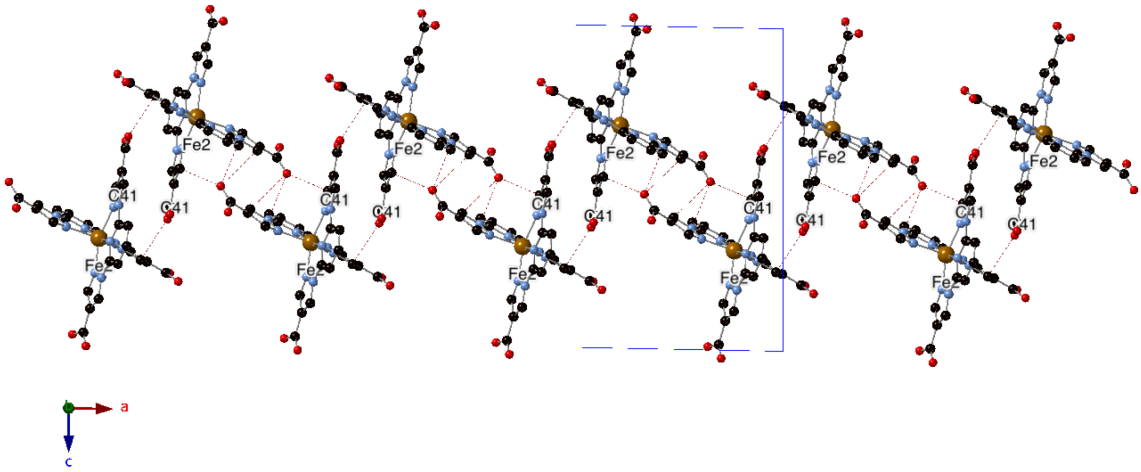

(c)

Fig. S7 Chains of $[Fe(bpCOOH_2p)_2]^{2+}$ complexes linked through intermolecular interactions (red-dashed lines) in the structure of **1** at 120 K (a) and 300 K (b and c).

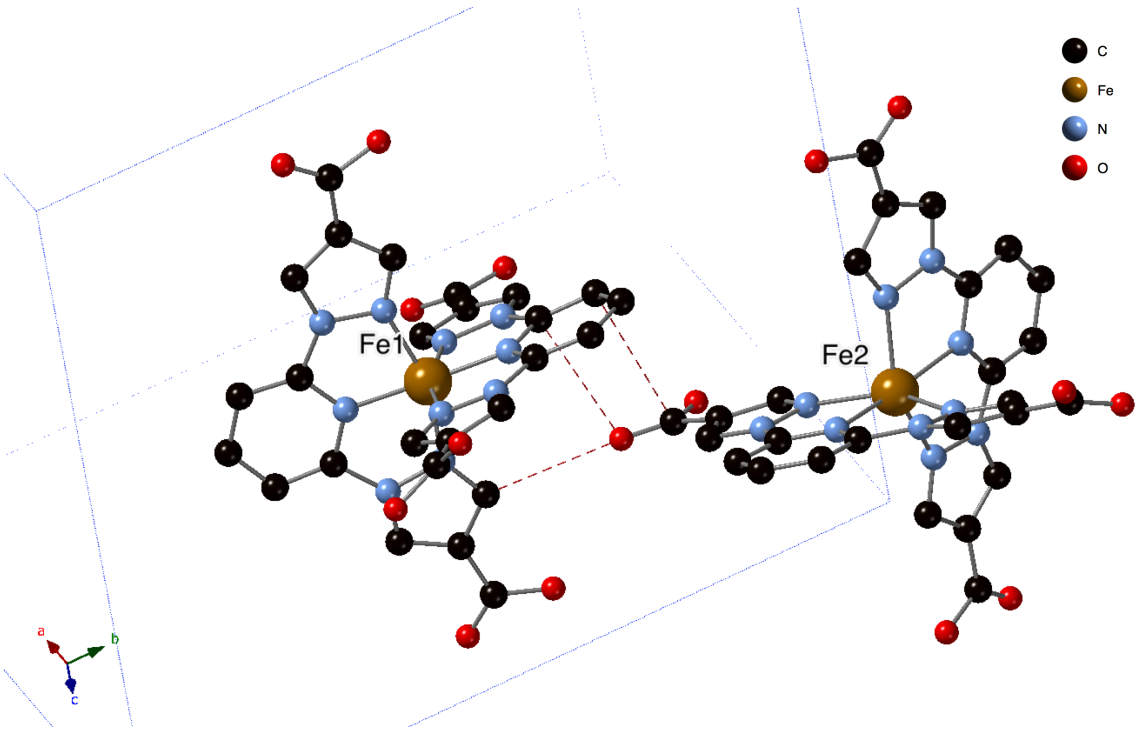

Fig. S8 Interchain interactions between $[Fe(bpCOOH_2p)_2]^{2+}$ complexes (red-dashed lines) in the structure of **1** at 300 K.

ESI. 7 Photomagnetism and theoretical evaluation of the kinetic relaxation.

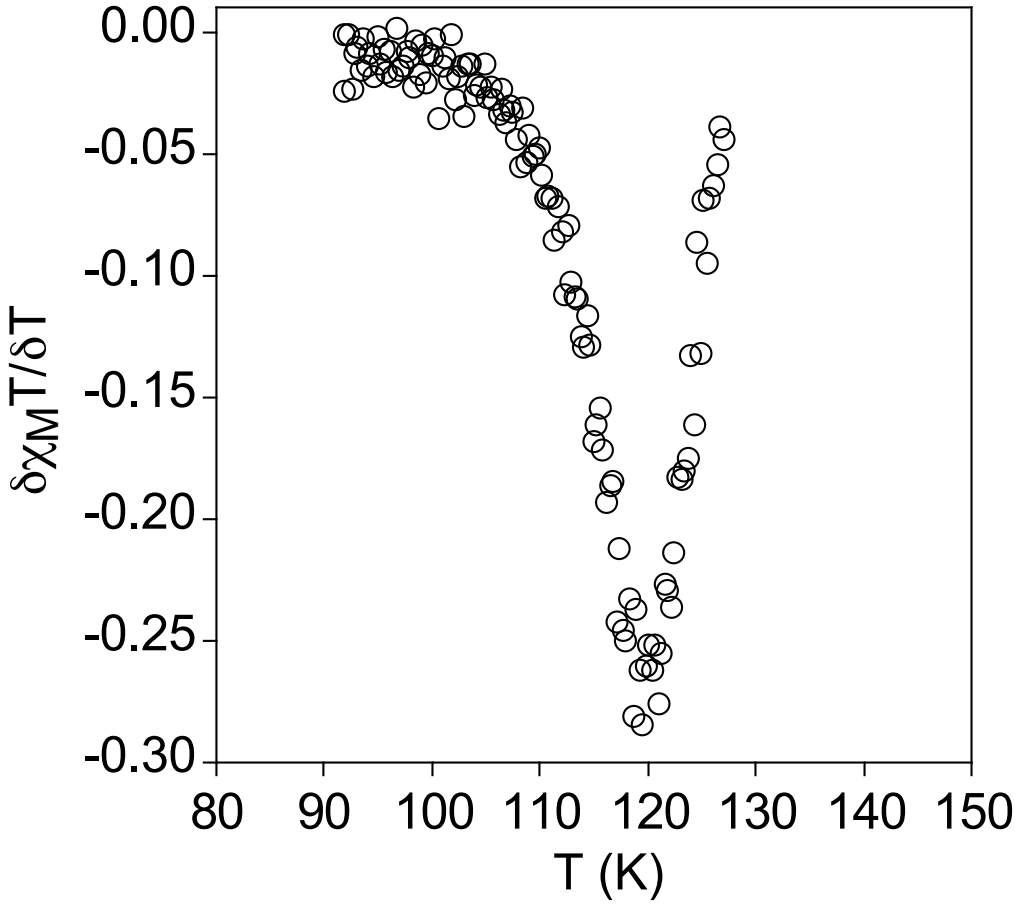

Fig. S9 Temperature dependence of the first derivative of $\chi_M T$ with respect to the temperature of **1** after light irradiation with red light.

In order to determine the kinetic mechanism that govern the magnetic relaxation of the photoexcited HS state we have used the model proposed by Hauser et al for a cooperative system.[7,8]

$$\frac{\partial \gamma_{HS}}{\partial t} = -k_{HL} * \gamma_{HS} \quad (1)$$

$$k_{HL}*(T, \gamma_{HS}) = k_{HL}(T)\exp[a(T)(1 - \gamma_{HS})] \quad (2)$$

$$\text{where } a(T) = E_a*/k_B T \text{ and } k_{HL}(T) = k_\infty exp(-E_a/k_B T)$$

Using these set of equations, we have programmed a IGOR Pro 8 (Wavemetrics software, Lake Oswego, OR, USA) procedure to perform the fitting of the photoexcited relaxation for a range of temperatures between 105 and 120K (see figure S10 left). These fittings run over two main parameters for each curve: $k_{HL}(T)$ and $a(T)$, with the boundaries of $k_{HL}(0)$. From the exponential definition of $k_{HL}(T)$, it is possible to define a typical Arrhenius law to extract the activation energy of the transition E_a and the preexponential factor k_∞ (see figure S10 right). In this latter case, the 105K measurement has been rejected due to the long relaxation rate at the measured times and the uncertainties in the extrapolation.

The values of the k_∞ and E_a obtained from these fittings are higher than those reported in the literature. Furthermore, the low value of E_a* could indicate a low level of cooperativity. However, these values have to be taken with caution since they are obtained with a limited number of experiments so they could be considered as preliminary. It was not possible to perform a complete set of relaxations at different temperatures for practical reasons, which are related mainly to the long irradiation times needed to reach saturation (8 hours). An additional problem is that it was not possible to reuse the same sample for relaxations at different temperatures. Thus, if the same sample was reirradiated after being heated above 120 K to erase the metastable state obtained in the first irradiation, slightly faster relaxations were obtained (see Fig. S11). This could be related to irreversible damage of part of the sample related to loss of solvent molecules or other structural changes. As a result of this, it was necessary to use a fresh sample for a relaxation at a given temperature.

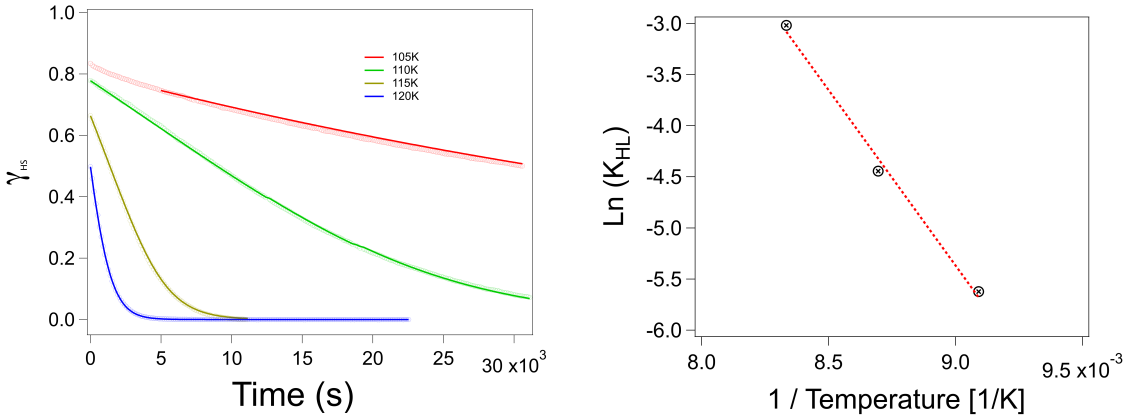

Fig. S10 (Left) Time dependence at various temperatures of the photoinduced HS molar fraction. The relaxation curves are fitted according to sigmoidal behavior (see text for more details). (Right) Arrhenius fitting of the activate process (the measurement at 105K has been removed from the fitting, see text).

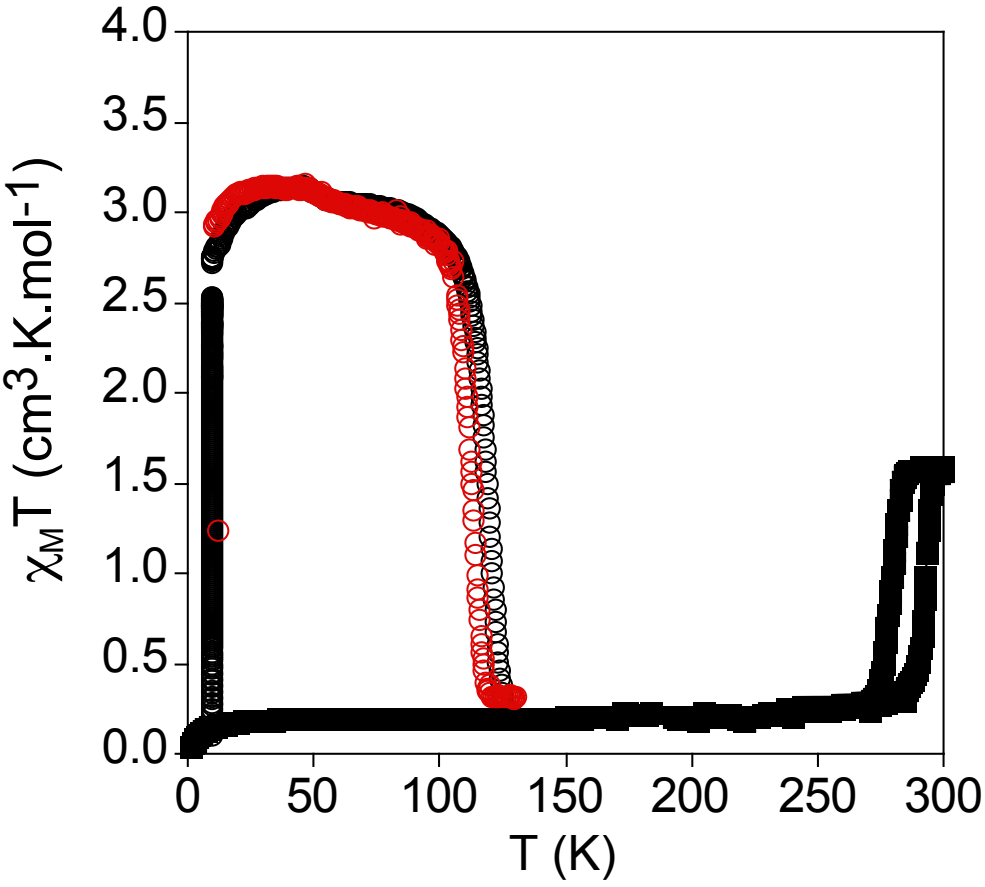

Fig. S11 Thermal dependence of $\chi_M T$ of **1**. Full squares: data recorded without irradiation; Black empty circles: data recorded after the first irradiation at 10 K and; Red empty circles: data recorder after second irradiation at 10 K.

ESI. 8 Structure and magnetic properties of 2.

The structure of $[Fe^{II}(bpCOOCOOHp)(bpCOOH_2p)Fe^{II}(bpCOOH_2p)(ClO_4)](ClO_4)_2{\cdot}H_2O{\cdot}1.5Me_2CO$ (**2**) at 120 K, which belongs the triclinic space group *P*-1 is formed by cationic chains of formula $[Fe^{II}(bpCOOH_2p)(bpCOOCOOHp)Fe^{II}(bpCOOH_2p)(ClO_4)]^{2+}{}_n$ separated by ClO_4^- counteranions and water and acetone, which in some cases are disordered (see Fig. S12). The asymmetric unit contains two iron atoms, two $bpCOOH_2p$ and one $bpCOOCOOHp^-$ ligands (see below), three ClO_4^- (one of them coordinated to iron), two acetone molecules (one of them with an occupancy of 0.5) and one water molecule. These polymeric chains are formed by two crystallographically independent iron centers (Fe1 and Fe2) with a different coordination environment. Fe1 is coordinated by six nitrogen atoms from two tridentate $bpCOOH_2p$ and $bpCOOCOOHp^-$ ligands with a distorted octahedral coordination geometry (Σ = 145.8(2)°, Θ = 478.3(5)°, ϕ = 173.85(19)° and θ = 81.8°) and typical HS Fe-N distances (2.105(5)-2.187(6) Å). We call $bpCOOCOOHp^-$ to partially deprotonated $bpCOOH_2p$. Thus, one of the two CO bonds of $bpCOOCOOHp^-$ presents very similar CO distances (1.243(8) and 1.254(8) Å), whereas the carbonyl C=O (1.247(8) Å) and alcoholic C−OH (1.290(9) Å) ends of the other carboxylic acid group can be distinguished. The other ligand linked to Fe1, $bpCOOH_2p$, presents distinguishable C=O (1.217(13) and 1.236(10) Å) and C-OH (1.269(14) and 1.308(10) Å). The O from the C=O group of the carboxylic acid end and one of the two O atoms from the carboxylate end of $bpCOOCOOHp^-$ are linked to two Fe2 leading to zig-zag chains running along the *c* axis. Therefore, $bpCOOCOOHp^-$ ligand acts as a bridging ligand to three iron ions. Thus, the carboxylate and carboxylic acid groups of the two sides are coordinated to two Fe2 ions, while the central pyridyl and the two pyrazolyl rings are coordinated to Fe1 in the usual tridentate way of bpp (see Fig. S12). The remaining four positions of the distorted octahedral coordination of Fe2 are completed with one oxygen from a ClO_4^- anion and one tridentate $bpCOOH_2p$ ligand with distinguishable C=O (1.232(9) and 1.238(9) Å) and C-OH (1.322(9) and 1.255(10) Å) distances. The O atoms belonging to perchlorate and carbonyl groups are in trans, while the carboxylate group is in trans to the N atom from the pyridyl ring. Moessbauer measurements need to be performed to confirm the oxidation state of Fe2. Fe-N and Fe-O distances in Fe2 are typical HS distances ranging from 2.147(6)-2.204(6) Å for Fe-N and 1.967(5)-2.223(6) Å for Fe-O as expected for a FeN3O3 coordination. Coordinating perchlorate group seems to be important for the stabilization of the structure, as attempts to obtain a similar compound with tetrafluoroborate were unsuccessful. The shortest Fe-O distance corresponds to the carboxylate group in agreement with the more ionic character of this bond.

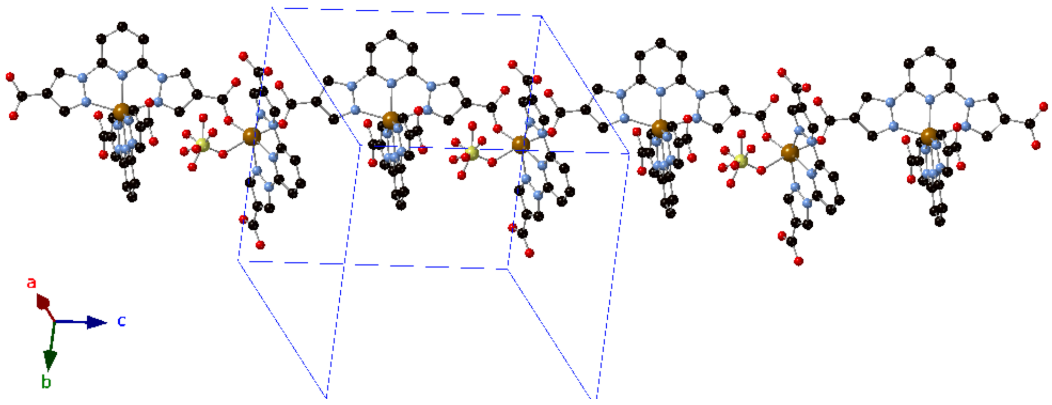

Fig. S12 Structure of the $[Fe^{II}(bpCOOH_2p)(bpCOOCOOHp)Fe^{II}(bpCOOH_2p)(ClO_4)]^{2+}{}_n$ chains in the structure of **2** at 120 K. Fe (orange) C (black), N (blue), O (red), Cl (yellow), H(white).

χ_MT of crystals of **2** measured in contact with the mother liquor shows a value of 6.8 $cm^3 \cdot K \cdot mol^{-1}$ at 220 K consistent with the two iron(II) complexes in the HS state found in the structure at 120 K. This value remains constant at lower temperatures with a decrease below 30 K due to zero-field-splitting (Fig. S13). Therefore, the magnetic interactions between iron(II) centers trough the bppCOOCOOHp$^-$ ligand seem to be negligible. The desolvated sample measured after heating to 400 K in the squid shows a continuous decrease of χ_MT from 400 to 80 K, which is more abrupt below 250 K. From 80 to 30 K, χ_MT reaches a constant value around 5.0 $cm^3 \cdot K \cdot mol^{-1}$ with the expected abrupt decrease below 30 K due to zero-field-splitting. The χ_MT values at 400 and 80 K (6.4 and 5.0 $cm^3 \cdot K \cdot mol^{-1}$, respectively) indicate that 25 % of iron(II) centers undergo a SCO in the desolvated phase. This corresponds roughly to half of the 50 % of the iron(II) centers coordinated to bppCOOH$_2$p and bppCOOCOOHp$^-$ ligands (with N6 coordination) since SCO is not expected for the remaining 50 % of iron(II) centers with a N3O3 coordination. Photomagnetic measurements were performed in this desolvated sample, since it is the one showing thermal SCO (see above). A drastic increase of the magnetic signal was observed after irradiation at 532 nm. χ_MT after irradiation reaches a maximum value of 6.0 $cm^3 \cdot K \cdot mol^{-1}$, which is close to the value obtained at higher temperatures before irradiation. Therefore, an almost complete photoconversion of the 25 % of LS iron(II) centers at 10 K is achieved. The T(LIESST) is close to 85 K, which in this case is consistent with the T(LIESST) vs. $T_{1/2}$ linear relationship with T_0 =150 K (see Fig. S13).

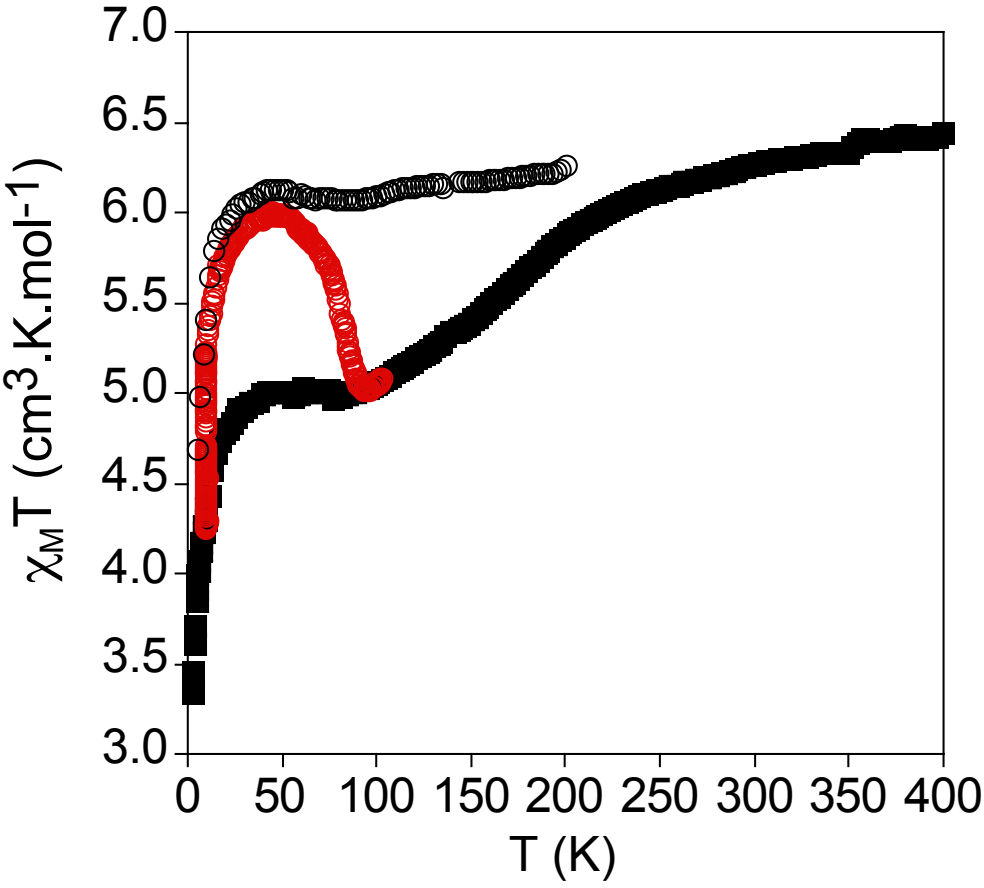

Fig. S13 Thermal dependence of χ_MT of **2**. Empty circles: Compound measured in contact with the mother liquor. Full squares: data recorded without irradiation after desolvation at 400 K; red empty circles: data recorded after irradiation at 10 K for the same desolvated sample.

REFERENCES

1 R. Pritchard, C. A. Kilner, S. A. Barrett and M. A. Halcrow, *Inorganica Chimica Acta,* 2009, **362**, 4365.
2 C. M. Amb and S. C. Rasmussen, *J. Org. Chem.,* 2006, **71**, 4696.
3 G. M. Sheldrick, *Acta Cryst.,* 2015, **A71**, 3.
4 G. M. Sheldrick, *Acta Cryst.,* 2015, **C71**, 3.
5 O. V. Dolomanov, L. J. Bourhis, R. J. Gildea, J. A. K. Howard and H. Puschmann, *J. Appl. Cryst.,* 2009, **42**, 339.
6 A. L. Spek, *J. Appl. Cryst.*, 2003,**36,** 7.
7 A. Hauser, *Chem. Phys. Lett.,* 1992, **192**, 65.
8 A. Hauser, J. Jectic, H. Romstedt, R. Hinek and H. Spiering, *Coord. Chem. Rev.* 1999, **190-192**, 471.